DESIGN AND PROPERTIES OF CEMENT COATING WITH MUSSEL SHELL FINE AGGREGATE

Martínez-García, Carolina[1]; González-Fonteboa, Belén[2]; Carro-López, Diego[3]; Martínez-Abella, Fernando[4]

[1]**PhD Student at the School of Civil Engineering**. Department of Construction Technology, University of A Coruña. **Postal Address**: E.T.S.I. Caminos, Canales, Puertos. Campus Elviña s/n, 15071 La Coruña, Spain. **E-mail**: carolina.martinezg@udc.es. **Telephone number**: (+34) 881015463. **Fax**: (+34) 981167170

[2]**Associate Professor at the School of Civil Engineering**. Department of Construction Technology, University of A Coruña. **Postal Address**: E.T.S.I. Caminos, Canales, Puertos. Campus Elviña s/n, 15071 La Coruña, Spain. **E-mail**: bfonteboa@udc.es. **Telephone number**: (+34) 881011442. **Fax**: (+34) 981167170

[3]**Associate Professor at the School of Civil Engineering**. Department of Construction Technology, University of A Coruña. **Postal Address**: E.T.S.I. Caminos, Canales, Puertos. Campus Elviña s/n, 15071 La Coruña, Spain. **E-mail**: dcarro@udc.es **Telephone number**: (+34) 881015429. **Fax**: (+34) 981167170

[4]**Professor at the School of Civil Engineering**. Department of Construction Technology, University of A Coruña. **Postal Address**: E.T.S.I. Caminos, Canales, Puertos. Campus Elviña s/n, 15071 La Coruña, Spain. **E-mail**: fmartinez@udc.es. **Telephone number**: (+34) 881011443. **Fax**: (+34) 981167170

Abstract

The production of farmed mussels amounts to millions of tonnes across over 40 countries. Shell waste resulting from this production has a very significant environmental impact. In Galicia, mussel shell waste is transformed, using low impact heat treatment, into a by-product that can be used as an aggregate. This research investigates cement-coating mortars where conventional aggregate is partially replaced with mussel shell aggregate. Reference mortars and mortars with mussel shell sand replacing conventional sand at different rates: 25%, 50% and 75% have been tested. Results show the feasibility of mussel shell in cement coatings at an optimal replacement rate of 25% of the conventional aggregate.

Keywords:

Mussel shell; cement coating; water vapour permeability; microstructure; porosity; workable life progression

Highlights:

- Mussel shells are a by-product converted into fine aggregate after a low environmental impact process

- Shell aggregate disturbs microstructure and pore size distribution of cement coatings
- Particle shape and shell composition are the main characteristics affecting coating properties
- The use of 25% mussel shell leads to accurate surface and base layer coatings

1 INTRODUCTION AND OBJECTIVES

Aquaculture and the cannery industry are important economic sectors in Galicia. They generate big profit and create thousands of jobs. However, they also produce lots of waste, including a remarkable volume of mussel shells. Galicia generates around 25,000t of mussel shell waste every year that is usually disposed of via landfill with great impact on the environment.

On the other hand, sand is one of the most-used natural resources in the world with the construction sector as its main consumer. Global aggregate production exceeds 50bnt (billions metric tons) every year [1], most of which comes from rivers, the bottom of the sea and beaches. In some countries, the aggregate used in mortar and concrete production has been obtained from quarries producing an obvious environmental impact, destroying natural habitats and transforming the landscape. Additionally, the aggregate production process carried out at quarry plants involves extraction, crushing, grinding and screening, inevitably leading to high energy consumption and contributing to CO_2 emissions.

According to the final estimates of the Spanish association ANEFA [2], in 2017 the construction sector reached a total consumption of 110.5 million tonnes of natural aggregate. To this figure we can add approximately one million tonnes of recycled aggregate and another half a million tonnes of artificial aggregate. Therefore, the total aggregates consumption in this sector reached 112 million tonnes. A significant volume of this aggregate (58%) is consumed in the mortar, concrete and precast industry. For this reason, this study attempts to incorporate mussel aggregate (a by-product from the canning industry) into this field.

Actually, different publications covering the feasibility of using seashells in mortar or concrete manufacture have increased in the last 10 years. Some of these works incorporate the seashells as aggregate in concrete [3–6], while other authors produce filler from the seashells and use it as a substitute for cement [7,8]. One recent work demonstrates the feasibility of using mussel shell as a source of calcium carbonate to synthesize belite rich cement using heat solid state activation [9]. There are also some studies that analyse the incorporation of oyster shells [10–12] or cockle shells or a mixture of seashells as aggregate in different kind of mortars [13–15]. Lastly, a work was found that incorporates seashells in cement mortars for masonry and plastering [16]. However, as a novelty, this study presents a detailed analysis of the microstructure of mussel shell mortars and studies how this microstructure can influence their properties. These new results will contribute to widespread the use of this material.

As stated in the literature, mussel shell is composed mainly of calcium carbonate and organic matter content that is located inside its microstructure. Mussel shells are formed by different layers and by an organic matrix composite that holds the layer structure together. The composition of the organic matrix composite are polysaccharides (chitin), proteins and glycoproteins [17,18], that can act as a setting retarder in cement systems. It is well known that the organic matter has different effects on cement mortar properties. Some authors [19] noted that organic matter can act as a retarder in cement mortars, increasing their workable life. Other works [20] show that the effect of the organic matter is similar to that of air entraining agents on cement mixes, introducing air voids into the cement paste.

Hence, this study aims to analyse the effect of replacing conventional aggregate with mussel shell in mortar production. The mussel shell used is heat treated before using this by-product as an aggregate.

Traditional coating mortars are applied in several layers that present different characteristics and purposes according to their thickness, composition or dosages and according to their position in the coating [21]. Different authors [22,23] suggest designing cement or lime-cement coating mortars in layers with different thickness and dosages regarding its position and the partition type. That is, the first layer (preparatory coat) is used to be an adherence bridge with a poorer dosage and even without aggregate, just like a paint. The next layer is a base layer that is usually designed with a low binder-to-aggregate ratio and with large aggregate size, which lead to high porosity. The following layers are made with higher binder content. The layer thickness is fixed by the aggregate size, the larger the aggregate size, the thicker the layer can be. Coating repairing is, usually, the reason that leads to make plasters in layers: the surface layer has to be repaired frequently, so that the base layer has to be well adhered and has to guarantee protection against moisture.

The mixes were designed in order to create two different coatings: base and surface layer coatings. Baseline coatings with conventional sand were compared to mussel shell mortars made using different replacement rates (25%, 50% and 75% by volume). Different fresh state properties were studied and, at hardened state, the microstructure and pore size distribution were analysed in order to further understand hardened behaviour.

2 MATERIAL AND MIXES

2.1 Cement and aggregate

The cement used was a masonry cement MC12.5-X (without air entraining agent). The cement composition was: portland cement (clinker 41.3%) and inorganic compounds (limestone 33.5%, calcined natural pozzolana 19.8%, gypsum 5.4%). Results of the X-ray Fluorescence (XRF) characterisation are shown in Table 1.

The sand used comes from a crushed limestone with a maximum size of 4 mm. From this sand, two different fractions were obtain by sieving. A fine sand (0-1mm-FNS) and a coarse sand that was obtained by combining different fractions of the original limestone sand (0-4 mm-NS) (Fig. 1).

Table 1. Chemical composition by XRF characterisation (%).

	MC12.5-X
CaO	48.5
SiO_2	17.9
Al_2O_3	6.1
Fe_2O_3	3.7
SO_3	3.5
MgO	1.5
K_2O	1.1
Na_2O	0.55
TiO_2	0.28
P_2O_5	0.069
SrO	0.064
ZnO	0.048
Cl	0.046
MnO	0.040
ZrO_2	0.034
CuO	0.022
LOI 550ºC	2.9
LOI 975ºC	16.5

The mussel shell supplied was heat-treated according to European regulation [24] (135°C for 32 minutes). The X-ray Fluorescence (XRF) characterisation of mussel shell shows that it is composed mainly of calcium carbonate (95%), and is formed by the bio-mineralisation of $CaCO_3$ with a small amount of organic matrix which holds the structure together, as shown in a previous work [18].

Two mussel shell sands, a coarse sand (0-4mm-CMS) and a fine sand (0-1mm-FMS) were supplied after applying a grinding and sieving process to the heat-treated mussel shell. Lastly, the mussel sands used were fine mussel shell sand (0-1mm-FMS) and mussel shell sand (0-4mm-MS) obtained from the mixture of the two supplied fractions to obtain a particle size distribution equivalent to that of the natural sand (NS). The mix percentages used were 88.5% of FMS and 11.5% of CMS (Fig. 2). Table 2 shows the natural and mussel shell sand properties.

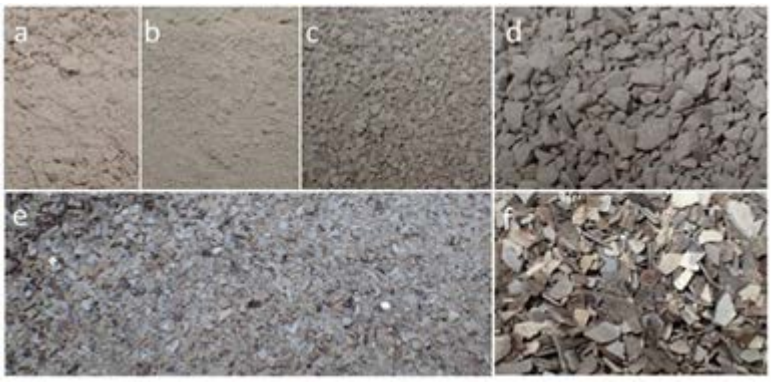

Fig. 1. Sand aggregates: a) Limestone sand 0-0.063mm b) Limestone sand 0.063-0.25 mm c) Limestone sand 0.25-1mm d) Limestone sand 1-4mm e) Fine mussel shell sand (FMS) 0-1mm f) Coarse mussel shell sand (CMS) 0-4mm

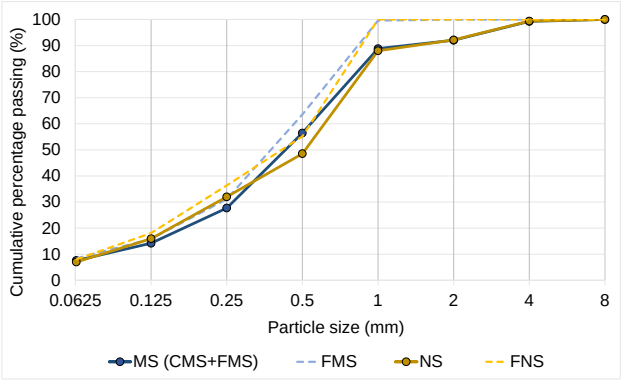

Fig. 2. Particle size distribution of aggregates

Table 2. Sands properties

	MS (11.5%CMS+88.5%FMS)	FMS	FNS	NS
Heat treatment	32min at 135˚C	32min at 135˚C	No	No
Sieve modulus	2.21	1.90	1.90	2.23
Particle density (kg/dm^3) [25]	2.72	2.73	2.67	2.67
Water absorption (%)[25]	3.94	4.12	2.22	2.22
Chlorides (1%) [26]	0.48	0.51	0	0
Soluble sulphates (%)[26]	0.59	0.59	0	0
Soluble sulphates (%)[26]	1.33	1.3	-	-
Organic matter (%)[27]	2.07	2.15	0	0
Sand equivalent (%)[28]	71.77	68.2	64	64

2.2 Mix design

Two different baseline mixes of coating mortars were designed. One was designed to be used in a base layer and the other in a surface layer. Mix proportions were chosen to ensure high enough workability so that high percentages of mussel shell sand could be incorporated.

The mortar dosage of the base-layer coating (BC) was designed with a cement:sand ratio of 1:5 (by volume) and a water:cement ratio of 1 (by weight). The dosage for surface-layer coating (SC) was designed with a cement:sand ratio of 1:4 and water:cement ratio of 0.9.

Mussel mortars were designed replacing conventional sand with mussel shell sand by volume. The replacement percentages used were 25%, 50% and 75%. So eight mussel shell cement mortars were obtained. Table 3 shows the mix proportions of the reference mortars and the mussel shell mortars.

Table 3. Baseline and mussel shell mortars (g per litre)

	Replacement rate (%)			
	0	25	50	75
Cement	312.02			

BC	Water		312.02		
	NS	1560.12	1170.09	780.06	390.03
	MS	0	397.33	794.67	1192.00
SC	Cement		366.25		
	Water		329.63		
	FNS	1465.01	1098.76	732.51	366.25
	FMS	0	373.11	746.22	1119.33

3 TEST METHODS

3.1 Mixing and moulding

The raw materials were mixed in order to obtain the different mortars. The mixing procedure was carried out according to UNE-EN 196-1: firstly, cement and water were blended for 30 seconds at low speed. Then the aggregate was added and mixed for 30 seconds at low speed and 30 seconds at high speed. The mixing procedure was then stopped for 90 seconds, the mixer walls were scrapped in the first 30 seconds and finally, mixing continued for 60 seconds at high speed. Different batches were made to determine the fresh and hardened state behaviour of each mortar.

In order to carry out hardened state tests, mortars were cast in prismatic moulds (40x40x160mm). According to UNE-EN 1015-11 [29], a manual compaction system with a 50g rammer was used to remove air bubbles and voids. Mortars were maintained in the moulds for 2 days before demoulding. All mortars were cured in a climatic chamber and both the temperature and relative humidity were fixed at 20 °C ± 2 and 60 ± 5%, respectively. Prismatic samples (40x40x160 mm) were used to measure hardened density [30], compressive strength [29]), water absorption by capillarity action [31] and weight loss and shrinkage [32].

3.2 Fresh state tests

In fresh state, air content, consistency and stiffening time were determined just after mixing. Air content test was carried out according to UNE EN 413-2 [33]. Consistency was measured using the flow table method and the penetration probe method, according to EN 413-2 [33]. The fresh density was calculated as the fresh mass of the mortar divided by the volume of the filled mould, using the average mass of all batches made. The workable life and stiffening time were determined according to UNE EN 1015-9 [34], using a specific device with a bradawl that pushes the fresh sample until the strength exerted exceeds 15N.

3.3 Microstructure

At the age of 3 and 28 days, different mortar samples were pre-consolidated by impregnation with resin under vacuum. Thin slices were cut to a thickness of approximately 20 microns. Then the samples were polished, covered with a glass slip and examined with LEICA DM750M optical microscopy. Specimens used for scanning electron microscopy (SEM) were dehydrated

and covered with gold in a Bal-Tec SCD 004 sputter coater. In addition, some samples were examined and photographed using a JEOL JSM-6400 Scanning Electron Microscope.

3.4 Porosity, pore distribution and water absorption

Porosity accessible to water was measured according to UNE 83980 [35] at 28 days. For this test, circular moulds with a diameter of 150mm and thickness of 20 mm were used. By means of a core-drill, at least three pieces of each mortar were taken from different samples of hardened cement mortars at 28 days to measure water absorption and porosity accessible to water. The samples were saturated under water for 24-48hs until the stable mass was measured. Subsequently, the samples were boiled for 5 hours. The test pieces were allowed to cool in water for at least 15 hours. The next day the samples were weighed on a hydrostatic scale. Density, water absorption and porosity both after immersion and boiling were calculated.

Other little pieces (2 to 3 g) of hardened samples at 28 days were used to measure the pore size distribution with a Mercury Intrusion Porosimetry (MIP). This test was performed using a Poremaster-60 GT mercury porosimeter, which automatically registers pressure (between 6.29 KPa to 410759.65 KPa), pore diameter in a range between 0.003 to 200 μm, intrusion volume, and pore surface area.

3.5 Water absorption by capillarity

The water absorption was determined using the capillarity test according to UNE EN 1015-18 [31] at 28 days. Three 40x40x160 mm samples of each mortar were used for this test. After drying them to constant mass (oven-dried at 60˚C), the four largest faces of the specimens were sealed using paraffin, and then they were broken into two halves. Test pieces (six samples of each mortar) were placed on a tray with the broken face turned down on four supports so that they did not touch the bottom of the tray. The samples were maintained immersed in water to a height of 5 to 10 mm from their bottom. The specimens were weighed at two intervals (10 and 90 min) and the weight gain due to capillary absorption was recorded. Data was used to plot a graph showing the weight gain per unit of specimen base area versus the square root of time. The slope of the line is the capillary absorption coefficient.

3.6 Mechanical strength

The compressive test was carried out on prismatic specimens 40x40x160 mm using a universal multi-purpose touch-screen compression/flexural MATEST S205N Unitronic 50 KN with Cyber-Plus evolution control. Specimens were tested according to UNE EN 1015-11 [29]. The test velocity selected for flexural strength was 0.02 KN/s and for compressive strength was 0.15 KN/s.

3.7 Weight loss and shrinkage

Weight loss and shrinkage tests were carried out according to UNE-EN 12808-4 [32]. Specific shrinkage moulds of (40x40x160 mm) were filled with cement mortar. The moulds were kept inside a plastic bag in a climatic chamber for 48 hours. Then, the specimens were demoulded and were placed on a three-point support system. They were maintained inside the climatic chamber during the entire testing period. The first shrinkage measurement was taken right after demoulding. Then shrinkage measurements were repeated at 3, 7, 28, 56, and 90 days from the kneading date. In parallel, on the same dates, the weight of different samples were recorded.

4 FRESH STATE PROPERTIES: RESULTS AND DISCUSSION

4.1 Consistency (flow table and penetration tests)

The consistency was measured using the flow table test and penetration depth device. Fig. 3 and Fig. 4 show the spread diameter and penetration depth in mm, respectively, according to the percentage of mussel shell sand used. As expected, the mussel sand particle shape (with a high percentage of flaky particles) leads to an increase in the water demand, thereby reducing the workability of mussel mortars.

The results indicate that the consistency measured by spread diameter increases with the incorporation of mussel shell similarly in both coating mortars (base-layer and surface-layer mortars). Spread diameter slightly increases up to a replacement rate of 25%, although the increments are noticeable from 25% on.

Regarding the penetration test results, they show that this test is more sensitive to mussel shell incorporation than the flow table test, in both BC and SC mortars, with this effect being more noticeable in the BC mixes. This is caused by the blocking effect of mussel shell aggregate flaky particles which occurs as the penetrating probe falls into the mortar. This is intensified in the base-layer mixes due to the use of larger-sized aggregate particles and a higher aggregate content.

These results are consistent with those obtained by other authors [16,36,37], which, in all cases, conclude that mixtures made with seashells as an aggregate reduce mortar workability.

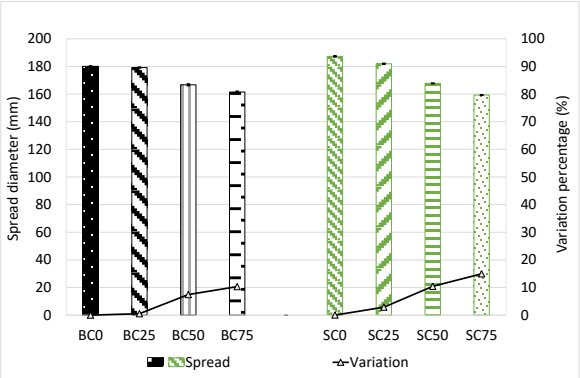

Fig. 3. Spread diameter.

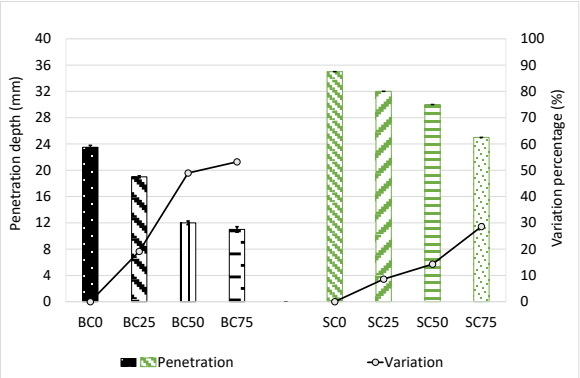

Fig. 4. Penetration depth.

4.2 Fresh density and air content

Fresh density and air content were evaluated in fresh state. As can be seen (Fig. 5 and Fig. 6), the density of cement mortars decreases significantly with the increase in the percentage of mussel sand used, with both coating mortars being affected in a similar way. The reductions are linear in the range of 15% to 30 % for replacement rates from 25% to 75%, in both BC and SC.

Air content results confirm this effect. Thus, the air content of the BC75 and SC75 is about 6 times higher than that obtained with their reference mortars, BC0 and SC0.

As the densities of both mussel shell sands (MS and FMS) are similar to those of the limestone sand, this density reduction is attributed to the irregular and flaky particle shape of the mussel shell aggregate and the organic matter content of its microstructure. This organic matter can act as an air entraining agent [38–41], producing an amount of air in the form of uniformly dispersed microscopic bubbles. This higher porosity in the mussel mortar leads to density reductions.

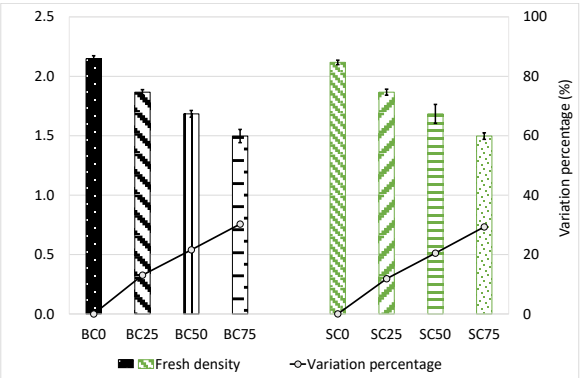

Fig. 5. Fresh density.

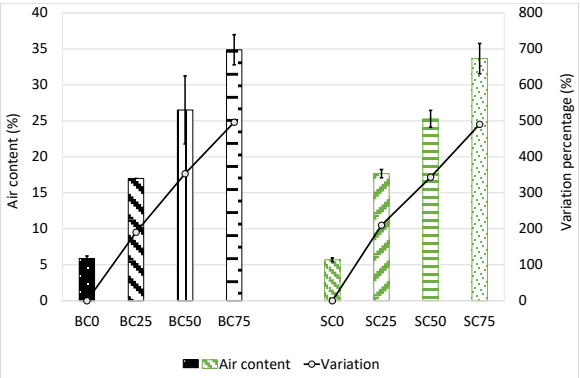

Fig. 6. Air content.

4.3 Workable life or stiffening time

Workable life or stiffening time of cement mortars is related to the setting time of cement pastes: a workable life increase indicates a delay in setting time. Fig. 7 shows the results of this parameter and it can be seen that mussel shell aggregate leads to an increase in the workable life of both coating mortars, with this increase being higher in the SC than the BC. The 25% replacement percentage hardly affects the stiffening time, resulting in increments of about 5% in both BC and SC. When 50% of mussel shell is used, the increments are significantly higher, 34% and 42.5% for both BC50 and SC50, respectively. With 75% of the conventional sand replaced, the base-layer mortar shows nearly a 90% increase and the surface-layer coating, SC75, reaches an increase of over 100%.

This delay in the setting time of mussel shell mortars is in agreement with results obtained in works carried out by other authors [16,42,43]. These works confirmed that the presence of seashell used as an aggregate (replacing conventional aggregate) or as ash (partially replacing the cement) in cement mortars or concretes delays cement hydration and increases the workable life of the mixes.

There are different kinds of retarders that carry out different mechanisms for the retardation of cement. These mechanisms are (1) formation of calcium complexes, (2) precipitation of insoluble compounds creating a semipermeable layer around cement particles, (3) direct surface adsorption of the retarder onto the clinker phase(s), and (4) adsorption on nuclei of C–S–H and portlandite, poisoning their formation and growth [44].

To be specific, the effect of saccharides on cement hydration is complex. Calcium chelating of organic retarders is significant, and the nucleation poisoning/surface adsorption of sugars is also evident. However, Kochova et al. also confirms that saccharides can interact with the main clinker minerals differently, for example, sucrose reacts with C_3S but does not react directly with C_3A and also accelerates ettringite formation, which is shown at early stages [19].

Therefore, it can be concluded that the delay in setting time detected in mussel shell mortars is due to the organic matter content and specifically to the presence of polysaccharides, as chitin in the shells.

Lastly, although mussel aggregate content is higher in the BC than in the SC, the increase in stiffening time due to the incorporation of mussel shell is higher in the surface-layer mortar than in the base-layer mortar. This is due to the fact that in SC mortars only the fine fraction of the mussel sand was used, with a high specific surface area, thereby enhancing the effect of chitin on the cement paste hydration.

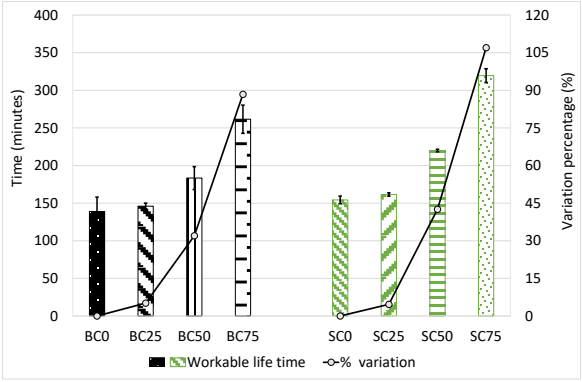

Fig. 7. Workable life progression.

5 HARDENED STATE PROPERTIES: RESULTS AND DISCUSSION

5.1 Microstructure

Fig. 8 and Fig. 9 show SEM images of both baseline mortars (BC0 and SC0) and both mussel shell mortars with a replacement percentage of 75% (BC75 and SC75).

At three days, the images show a microstructure with a lower porosity in both baseline mortars (Fig. 8a and Fig. 8d) than in the mussel shell mortars. The structure shown in Fig. 8b (BC75) and Fig. 8e (SC75) presents small and numerous pores, showing a microstructure similar to that formed when air entrainment additives are used [20,45]. These air entrained pores are rounded voids formed by the organic compounds present in the shell structure. Different authors [46–49] suggest that sulphated compounds and S-containing amino acids are associated with intercrystalline structures and the intracrystalline organic matrix of mollusc shells.

Micrographs also show smooth areas with an elongated and concave shape in the cement paste of mussel shell mortars. It is likely that these areas correspond to the region of cement paste around the shell particles, denoting a poor paste-aggregate bond when these aggregates are used. In addition, this contact area also presents high porosity, confirming, again, that mussel shell aggregate produces high cement paste voids.

In Fig. 8c (corresponding to BC75) the interfacial transition zone (ITZ) between the cement paste and a large size mussel shell particle at 28 days can be seen. This image confirms a significant lack of bond between the shell particle and the cement matrix, and shows an ITZ with a significant crack width. Additionally, many cracks can be seen throughout the mussel particle and cement paste. Fig. 8f presents the paste microstructure of SC75, showing both rounded and irregular large pores generated by the mussel fine particles. Again, in this case, many cracks are observed throughout the cement paste.

In Fig. 9 imaging magnification of 5000x is used to present the microstructure of SC0 and SC75 mortars at 28 days. In this figure, the ettringite formation can be seen. In the baseline surface layer coating almost no ettringite needles are seen whereas in the SC75 sample the ettringite crystals are clearly seen forming small networks.

Chitin is a large structural polysaccharide made from chains of modified glucose monosaccharides. It is formed by a series of glycosidic bonds between substituted glucose molecules. Actually, chitin may be considered a natural polysaccharide compound of residues of b-1,4-N-acetyl-D-glucosamine.

In this regard, it is known that monosaccharides or sugar acids retard cement hydration [50–52]. However, their effect is complex and explained by different phenomena. General studies about organic retarders have shown that they have strong Ca chelating groups which can prevent C-S-H gel formation [53–56]. Another effect is that sugars act through nucleation poisoning/surface adsorption forming semipermeable layers on the cement grains.

However, retarders interact differently with the clinker minerals, for example, sucrose reacts with C_3S but does not react directly with C_3A and also accelerate ettringite formation [57]. Actually, sucrose and the lignosulfonate accelerate ettringite formation but retard C_3S hydration. Ortega et al study the hydration of C_3A with excess gypsum with either sucrose or lignosulfonate. The results reveal an acceleration in ettringite formation, and the amount of ettringite continues to increase with time. Other studies [58] indicate that the interaction of sugars with C_3A prevents rapid formation of the cubic phase C_3AH_6 and promotes formation of the hexagonal phase C_4AH_{13}.

In this work, ettringite formation appears to be greater in the cement-chitin system than in the reference samples as was already seen by other authors. Some specific studies state that in the cement–chitin system, ettringite formation appears to be greater than in the reference samples [57].

Lastly, images also show that SC75 (Fig. 9b) presents less interparticle connectivity and less compactness than its corresponding baseline mortar. Also, a greater number of voids and worse redistribution of the cement matrix can be seen in SC75.

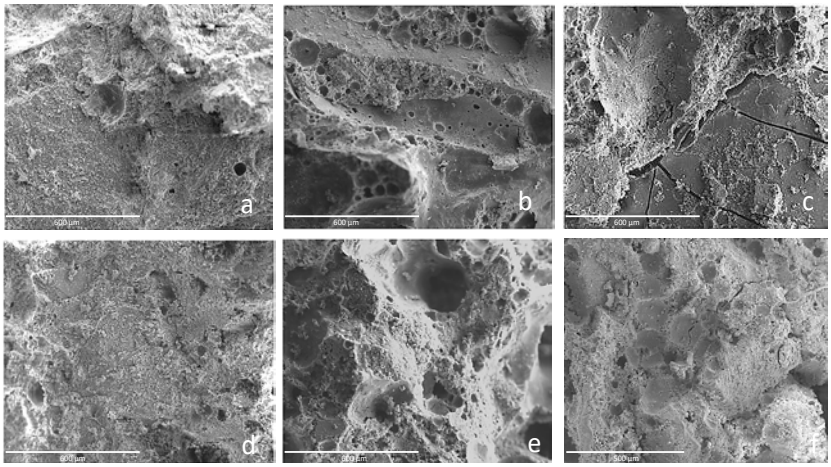

Fig. 8. SEM images (100x) of cement mortars: a)BC0 at 3 days, b)BC75 at 3 days and c)BC75 at 28 days, d)SC0 at 3 days, e)SC75 at 3 days and f) SC75 at 28 days.

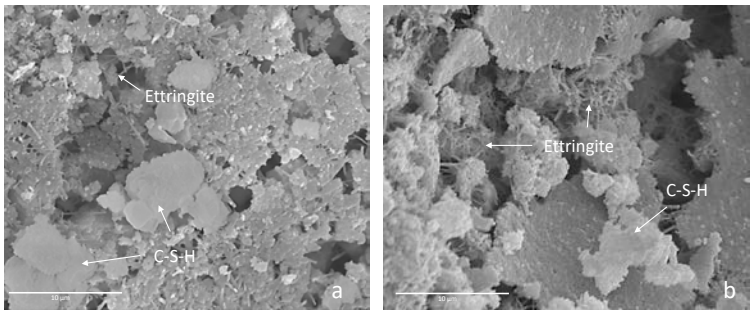

Fig. 9. SEM images (5000x) of cement mortars: a) SC0 at 28 days, b) SC75 at 28 days.

Optical microscopy photographs were used to measure pores larger than 200 microns that are not detected with mercury porosimetry (Fig. 10 and Fig. 11). Fig. 11 shows surface-layer mortar and it can be seen that large pores (above 300 µm) appear just from replacement rates of 25%. When mussel shell sand is used, this mortar shows irregular pores larger than the pores seen in the base-layer mortars (Fig. 10). Moreover, sometimes, these pores connect different mussel aggregates.

Additionally, the cement paste surrounding the mussel shell sand presents lots of small round pores, like those generated by entrapped air during mixing, although they display an irregular distribution in the paste. Again in this case, pores are less numerous in the base layer mortar. Lastly, cracks are also seen within the largest mussel aggregate particles of both mortar types.

All these results lead to the conclusion that mussel shell considerably increases mortar porosity. In addition to the air volume generated, it has to be taken into account that this porosity creates countless ITZ between pores and paste that will also affect mortar properties. Fig. 12 shows the ITZ generated in a large air void of BC50 and BC25 coatings. Most of the large air voids are going to present a similar structure. Other authors [59] state that air voids due to air entrainment present two distinct features: shell facing the air void surface and an interfacial transition zone between this shell and the bulk cement paste. Furthermore, the paste around the voids has a higher water content than the paste farther away from the interface. According to Piasta and Sikora [60], the interfacial paste of the porous microstructure occupies a large part of the cement paste volume. The air void interfaces can even overlap and interconnect. Therefore, mussel shell aggregate generates countless porous ITZ that will undoubtedly affect mortar properties.

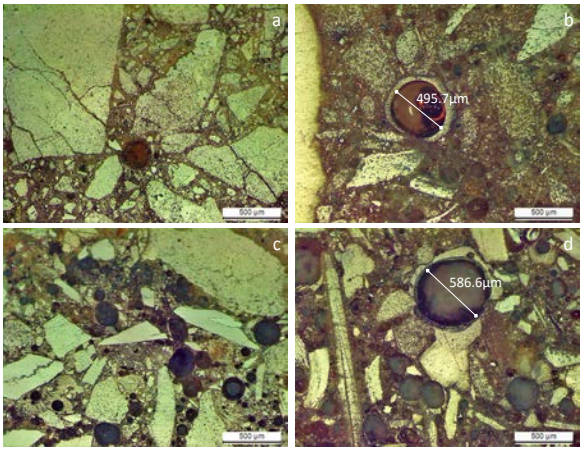

Fig. 10. Optical microscopy images of base layer coatings: a)BC0; b)BC25; c)BC50; d)BC75.

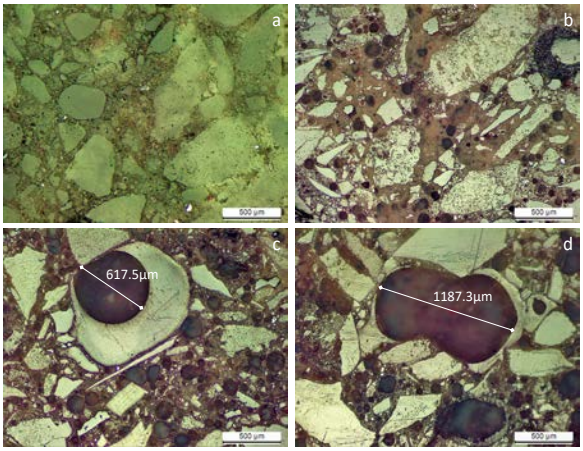

Fig. 11. Optical microscopy images of surface layer coatings: a)SC0; b)SC25; c)SC50; d)SC75

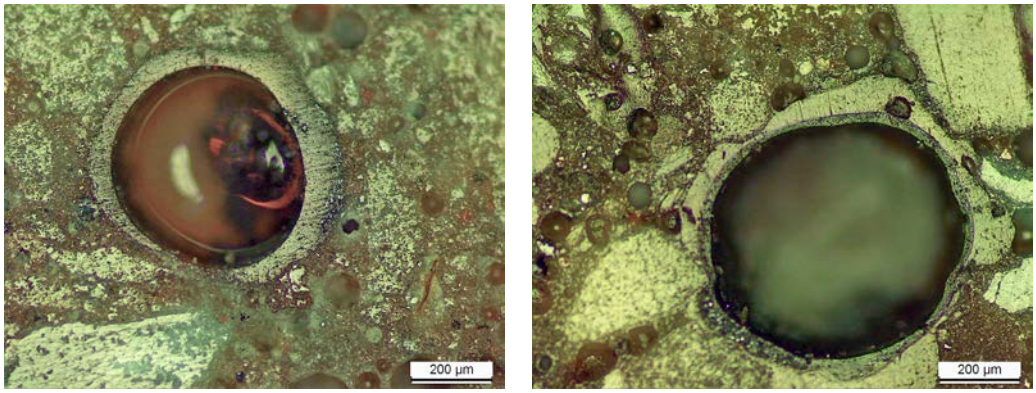

Fig. 12. Pore ITZ of BC25 (left) and BC50 (right)

5.2 Pore size distribution

Total porosity and pore size distribution of all mortar was measured with MIP using samples with a mass between 0.5 and 0.8 cm^3. The results confirm that mussel shell aggregate increases the porosity of cement mortars.

Fig. 13 shows the total porosity values. These values indicate that porosity is 7% higher in BC25 than in BC0. This increment is about 60% when BC75 is analysed. In the surface layer mortar, the increments are higher: 55% and 112% in SC25 and SC75 respectively when compared to SC0. These results confirm that small mussel shell particles (used in surface layer mortar) affect porosity to a higher extent than large mussel shell particles (used in base layer mortar).

The pore size distribution of the different mortars is shown in Fig. 14 and Fig. 15. It can be seen that the incorporation of mussel shell sand modifies the pore size distribution in the mortars. This is notable when the replacement ratio of conventional sand with mussel shell sand exceeds 25%. Up to 25%, mussel shell mortars present a pore size distribution that, although it displays a high volume of large pores, is slightly similar to the pore distribution of the reference mortars. However,

when 50% and 75% replacement rates are used, the pore size distribution of mussel mortars is considerably different from the distribution of the baseline mortars.

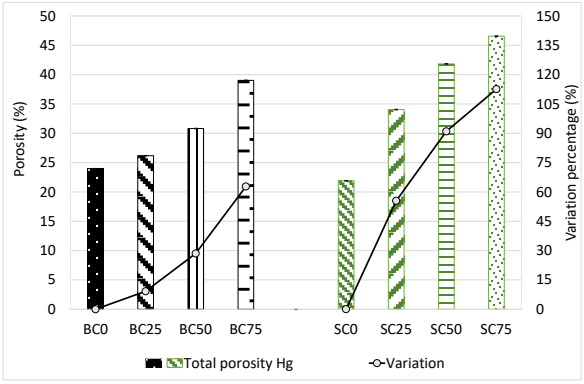

Fig. 13. Total porosity of cement mortars measured with Mercury Intrusion Porosimeter at 28 days.

Analysis of the curves leads to the conclusion that the incorporation of mussel shell aggregate significantly increases pore volume and generates many pores with a large diameter. In this regard, all curves move towards the right side of the graph. This indicates that the pore volume of large size pores (in the range of 1 to 100 µm) significantly increases while the pore volume of small size pores (in the range of 0.01 to 0.3 µm) slightly decreases (50% and 75% replacement ratios) or is maintained (25% replacement rate).

Lastly, these curves show, again, that BC0 and SC0 mortars present similar pore volume and similar pore distribution. However, the incorporation of small sized mussel shell particles in surface layer mortars leads to an increase in pore volume, mainly the pore volume of large size pores, and to a greater extent than with large sized mussel shell particles in base layer mortars.

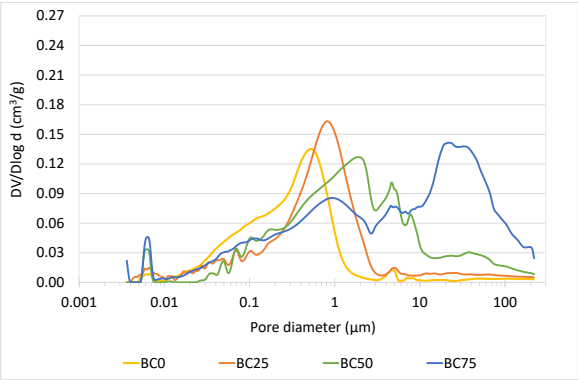

Fig. 14. Pore size distribution of base layer cement mortars.

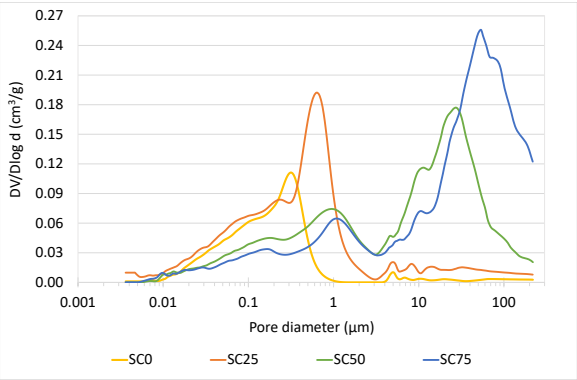

Fig. 15. Pore size distribution of surface layer cement mortars.

To further understand the pore size distribution, different pore ranges were analysed (Fig. 16). According to Gong et al.[61], the porosity of cement mortars is divided into three ranges: micropores, between 0.001 and 0.1µm (usually measured by

nitrogen and water adsorption methods), mesopores between 0.1 and 10 µm (sensitive to MIP method and image analysis) and macropores from 10 µm to 1 cm (detected by image analysis).

Analysing these ranges, Fig. 16, it is observed that, at any range, BC0 and SC0 mortars present similar pore volume. Only when micropores are analysed, does the SC0 mortar present higher percentage values than the BC0 mortar. Pores under 80 nm in diameter are usually ascribed to the gel and capillarity pores of the CSH structure [7]. Therefore they are more numerous in SC mortars (designed with higher cement content) than BC mortars.

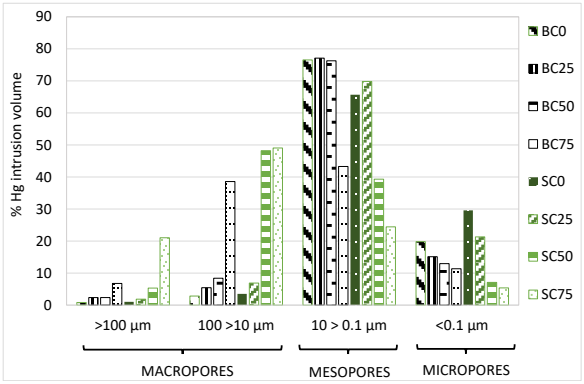

Fig. 16. Pore size ranges of cement mortars.

This analysis confirms again that the volume of micropores and mesopores decreases when mussel shell sand is used, especially when replacement percentages exceed 25%. As with baseline mortars, SC25 presents a higher micropore percentage than BC25. The volume of the mesopores tends to decrease as the mussel shell content increases, especially in BC75 when replacement percentages exceed 25% and the surface layer coating is analysed. Lastly, macropores increase significantly at a replacement rate of 75% in both coatings, although the increment is higher in the surface layer coating.

This pore size distribution is in agreement with the micostructure. It is clear that using mussel shell as sand aggregate leads to higher cement matrix porosity. The irregular shape of the particles and the presence of chitin in the mussel composition introduces large pores and damages the ITZ, thereby reducing the bond between the binder and the mussel aggregate (which is also related to the presence of large pores in the matrix [62]). On the other hand, the increase in ettringite formation may be filling small paste pores (< 0.1 µm), which was already seen by Ballester et al. [7].

5.3 Hardened density and porosity accessible to water

Fig. 17 shows hardened density of cement coatings at 28 days. Hardened density of cement mortars decreases with the incorporation of mussel shell sand. As observed with other properties, the influence of mussel shell on hardened density is similar in both the surface and base layer coating. Replacement rates of 25% lead to a decrease in the range of 10 - 12%, when 50% of conventional sand is replaced the reductions are about 20%, and when 75% of mussel sand is used the hardened density is 25-30% lower than that measured in the baseline mortars.

Fig. 18 shows porosity accessible to water after immersion and after immersion and boiling. In agreement with previous results, porosity is higher in mussel mortars than in baseline mortars. Additionally, results show that porosity values of all cement mortars are higher after water boiling than after water immersion, with a more noticeable difference in mussel shell mortars than in baseline mortars. This highlights the fact that air bubbles (that may not be well communicated) are part of the porous structure of mussel mortars. It is when boiling the samples that most of the total open porosity is filled with water.

Furthermore, due to the pressure applied, usually porosity measured with MIP is somewhat higher than that measured with the water penetration test [63]. However, in this work, results show that when replacement rates of 50% and 75% are used, the boiling water porosity is higher than the MIP porosity in both the surface and base layer mortars. The high volume of large pores (>500μm), not measured with MIP, justifies these results.

Fig. 19 shows the relationship between porosity after boiling water and hardened density at 28 days. It is clear that hardened density is directly related to porosity and, therefore, the mechanisms affecting the former are the same as those influencing the latter.

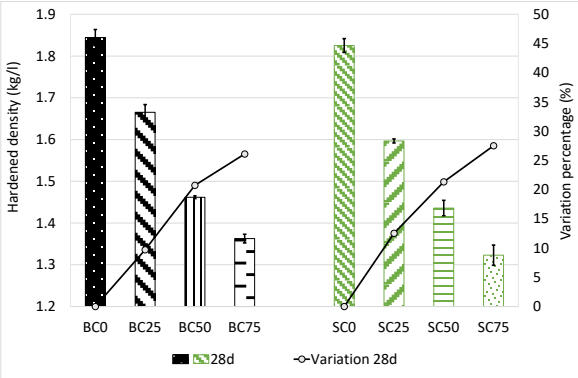

Fig. 17. Hardened density of cement coatings.

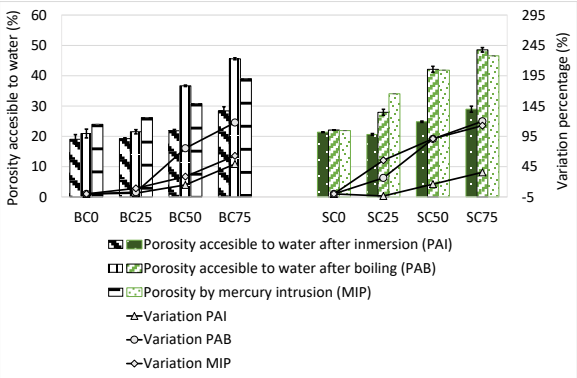

Fig. 18. Porosity of cement coatings.

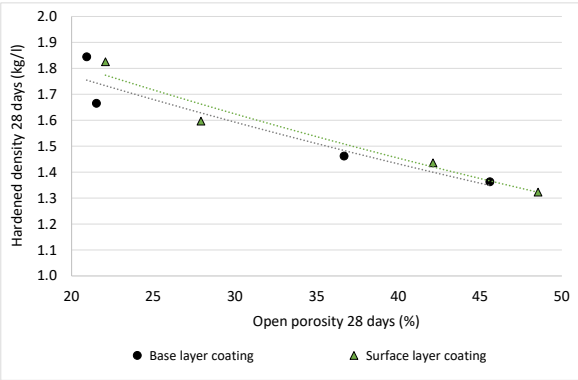

Fig. 19. Hardened density vs. porosity accessible to water at 28 days.

5.4 Water absorption

Fig. 20 shows water absorption at 28 days. These water absorption values are directly related to open porosity. Therefore, as occurs with porosity, water absorption is higher in mussel mortars than in baseline mortars. Additionally, water absorption after boiling is higher than after immersion. Again, the results confirm that small mussel shell particles (used in surface layer mortar) affect water absorption to a higher extent than large mussel shell particles (used in base layer mortar).

Lastly, in agreement with other results obtained in this work and found in the literature [37], the use of high replacement percentages (50% and 75%) significantly affects this property. However, when only a replacement rate of 25% is used, water absorption of mussel mortars is only slightly higher than that measured in baseline coatings. Air entrainment or entrapment produced by mussel shell organic matter content, the flaky shell shape and the low bond between the mussel shell and the cement paste, generates large pores that increases the mussel coating water absorption.

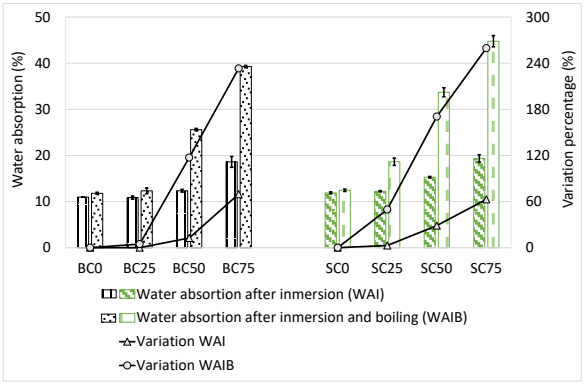

Fig. 20. Water absorption at 28 days.

5.5 Capillary uptake

Fig. 21 shows the water absorption due to capillary action measured at 28 days between 10 and 90 minutes. The results indicate that mussel shell aggregate decreases the capillary uptake of cement mortars. Once again, the effect of mussel shell sand is slightly higher in surface layer coatings than in base layer coatings. The reductions (using the corresponding baseline mortar as reference) are about 40% when the 25% of mussel aggregate is used (BC25=38%, SC25=43.5%) and almost 70% in BC75 (68%) and SC75 (67%).

According to the requirements established in UNE-EN 998-1 [64] for capillary absorption in rendering mortars, all mortars (but BC75 and SC75) can be classified as W0. Furthermore, mortars with 75% of mussel aggregate can be classified as W1 ($\leq$0.40 kg/m^{2}min$^{0.5}$), which allows them to be used as thermal insulation coatings.

The water absorption due to capillary action depends, not only on the total mortar porosity, but also on the mortar pore size distribution [65]. As seen in section 5.2., capillary pores (micropores and the small mesopores) are lower in mussel shell coatings than in baseline coatings, with the volume of large pores (>500µm) being higher in the former than in the latter. This issue combined with the particle shape of mussel shells (elongated and with large smooth surface areas) acts as a barrier to capillary water ascension.

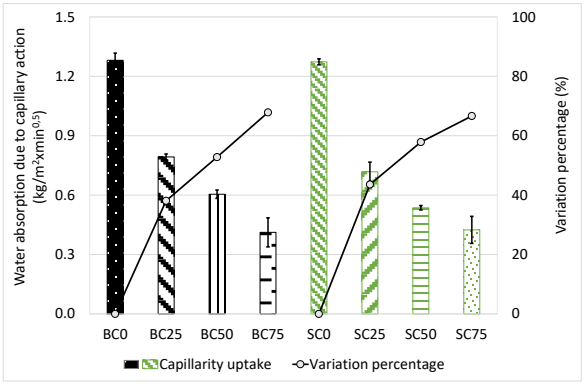

Fig. 21. Water absorption coefficient due to capillary action at 28 days.

5.6 Mechanical strength

Although mechanical strength is not a required property in coating mortars, its analysis leads to a deep understanding of the behaviour of mussel shell mortars. Compressive and flexural strengths are shown in Fig. 22 and Fig. 23.

In agreement with previous results, it can be stated that the use of mussel shell aggregate reduces mechanical strength. The reduction is similar in both compressive and flexural strength at any age (3, 7 and 28 days) and is also similar in both surface and base layer coatings.

The irregular and flaky particles of the mussel sand introduces large pores. Besides, the presence of chitin in mussel composition damages the ITZ, thereby reducing the bond between the binder and the mussel aggregate. This leads to a reduction in mechanical strength as the mussel shell sand content increases. Other authors have already stated that the use of seashell aggregate in cement mortar decreases its compressive strength [10,11,37,66,67]. The particle shape of the seashell aggregate (with large smooth surface areas and sharp edges) is the main feature affecting this property. Wang et al. [12] added fly ash to oyster shell mortar to counteract the effects of the shell aggregate resulting in an increase in compressive strength.

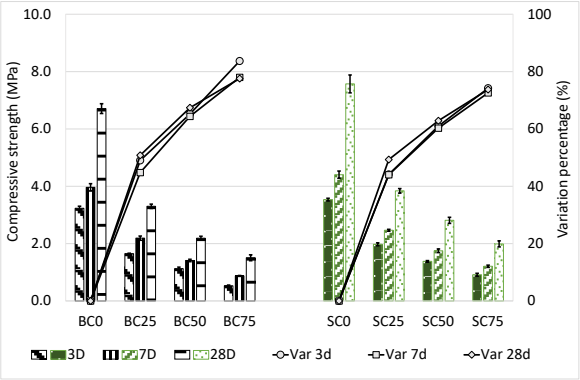

Fig. 22. Compressive strength at 3, 7 and 28 days.

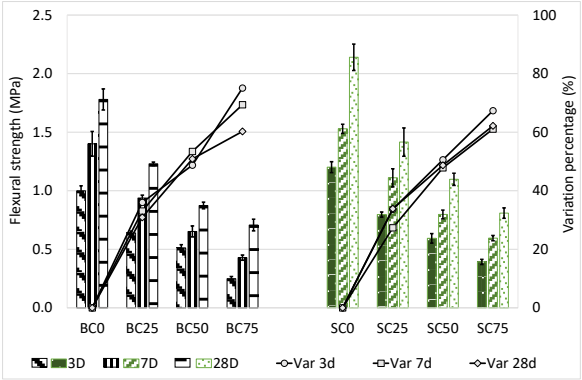

Fig. 23. Flexural strength at 3, 7 and 28 days.

5.7 Weight loss and shrinkage

Fig. 24 and Fig. 25 show results of weight control from the age of demoulding up to 90 days. It is observed that weight loss is lower in mussel shell mortars than in the reference mortars, in both surface and base layers coatings. In addition, similar weight loss was measured, regardless of the replacement percentage used. The low weight loss of mussel mortars may be due to the blockage of water migration caused by the particle shape of mussel shells.

However, although weight loss is lower in mussel shell mortars, their drying shrinkage is higher (Fig. 26 and Fig. 27). In this case, the shrinkage grows with the percentage of mussel shell used. Different authors [16,68] attribute this increase to the less-dense internal structure generated by the introduction of seashell aggregate: higher pore volume and weaker ITZ produce an increase in shrinkage. Also the organic matter content and the presence of chitin protein in the mussel composition leads the shrinkage to increase, as already detected by other authors [65,69–71].

Therefore, it can be stated that the blockage of water migration does not counteract the worse cement matrix generated with the use of mussel aggregate.

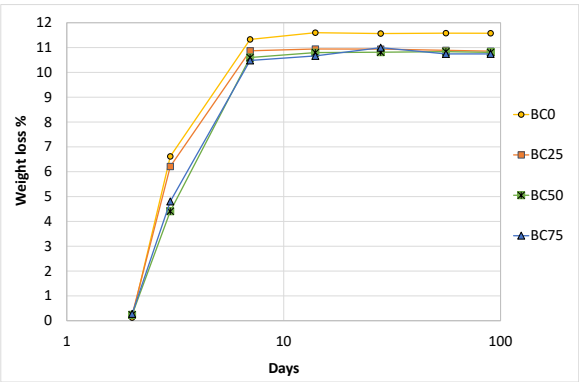

Fig. 24. Weight loss of base layer coating.

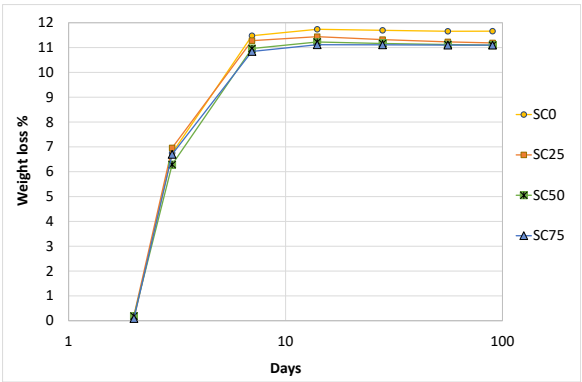

Fig. 25. Weight loss of surface layer coating.

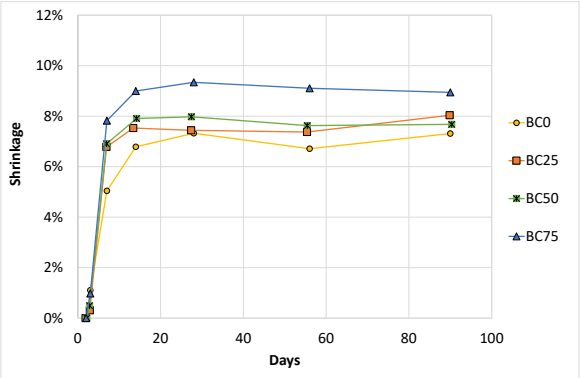

Fig. 26. Drying shrinkage of base layer coating.

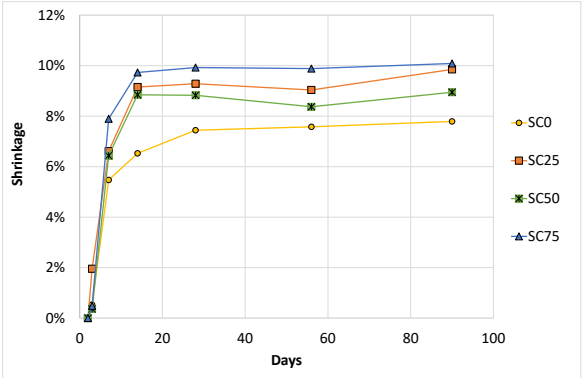

Fig. 27. Drying shrinkage of surface layer coating.

6 CONCLUSIONS

This work aimed to investigate the potential use of a by-product from the canning industry, mussel shell aggregate, in the production of cement coatings. Two different mixes of cement mortars were designed: a base layer coating and a surface layer coating. Mussel mortars were designed replacing conventional sand with mussel shell sand. The replacement percentages used were 25%, 50% and 75%, by volume, and the behaviour of the new mixes was compared to the behaviour of the baseline mortars.

- The organic matrix composite (polysaccharides, proteins and glycoproteins) that holds the layer structure together forms the mussel shell structure. Subsequently, one of the main conclusions reached in this work is that this mussel shell structure significantly affects cement mortar behaviour.
- Flaky particles and organic matter content behave like an air entraining agent. This increases air content, thereby decreases the fresh density and increaes the consistency of mussel shell mixes.
- The presence of polysaccharides (chitin) in mussel shell particles delays cement hydration, thereby increasing the workable life of mussel mortars. The higher specific surface area of the fine mussel sand affects slightly more to the surface layer coating.
- The irregular and flaky particles of the mussel sand introduce large pores in cement paste and reveals a lack of bonding between the shell particle and the cement matrix, that produces an increase in porosity and water absorption. However, on the contrary, the high volume of large pores (>500µm) combined with the particle shape of mussel shells (elongated and with large smooth surface areas) act as a barrier to capillary water ascension, thereby reducing the capillary uptake.
- Regarding mechanical strength, the existence of chitin in mussel composition considerably damages the ITZ reducing the bond between the binder and the mussel aggregate. This leads to a significant reduction in mechanical strength as the mussel shell sand content increases, again the effect is slightly higher in surface layer coatings.

- Moreover, particle shell shape blocks water migration causing a little decrease on weight loss of mortars. However, the weak ITZ and the high pore volume introduced by the use of mussel aggregate cause an increase in the drying shrinkage. The blockage to water migration does not counteract the worse cement matrix generated with the use of mussel aggregate. The higher increases in shrinkage were measured in the surface layer coating (higher specific surface area) than in the base layer coating.

Lastly, form the results obtained in this work, it can be stated that a replacement ratio of 25% of crushed limestone aggregate with mussel shell aggregate can be used to produce accurate surface and base layer coatings. This combined with the low energy consumption of the heat treatment used to produce the mussel shell aggregate, proves that the production of cement coatings with this canning industry by-product is a suitable and sustainable solution.

7 ACKNOWLEDGEMENT

This work has been carried out within the framework of the project "Valorización de las conchas de bivalvos gallegos en el ámbito de la construcción" (Assessment of Galician bivalve shell in the construction sector; Code 00064742 / ITC-20133094), funded by CDTI (Centro para el Desarrollo Tecnológico e Industrial) under the FEDER-Innterconecta Program, and co-financed with European Union ERDF funds. We wish to express our most sincere thanks to the professionals of the firms Extraco, Serumano and Galaicontrol.

8 REFERENCES

[1] European Aggregates Association, GAIN – Global Aggregates Information Network, Http://Www.Uepg.Eu/Media-Room/Links/Gain-Global-Aggregates-Information-Network. (2017). http://www.uepg.eu/media-room/links/gain-global-aggregates-information-network (accessed 11 December 2018).

[2] ANEFA, Official web of ANEFA, El Consum. Áridos Creció Un 10,5% En 2017, Hast. Los 112 Millones Toneladas. (n.d.). http://www.aridos.org/el-consumo-de-aridos-crecio-un-105-en-2017-hasta-los-112-millones-de-toneladas/ (accessed 4 December 2018).

[3] K.H. Mo, U.J. Alengaram, M.Z. Jumaat, S.C. Lee, W.I. Goh, C.W. Yuen, Recycling of seashell waste in concrete: A review, Constr. Build. Mater. 162 (2018) 751–764. doi:10.1016/j.conbuildmat.2017.12.009.

[4] K.H. Mo, U.J. Alengaram, M.Z. Jumaat, S.P. Yap, S.C. Lee, Green concrete partially comprised of farming waste residues: a review, J. Clean. Prod. 117 (2016) 122–138. doi:10.1016/J.JCLEPRO.2016.01.022.

[5] S.D. Halim, E. Rainer, C. Ryantonius, B. Panandito, D. Wardoyo, M.R. Fahlevy, I.S. Darma, The use of hazardous sludge solidification and green-lipped mussel shells in cementitious material: a case study of ngcc power plant of priok, MATEC Web Conf. 147 (2018) 01008. doi:10.1051/matecconf/201814701008.

[6] B. Lejano, Optimization of compressive strength of concrete with pig-hair fibers as fiber reinforcement and green mussel shells as partial cement substitute, Int. J. GEOMATE. 12 (2017). doi:10.21660/2017.31.6528.

[7] P. Ballester, I. Mármol, J. Morales, L. Sánchez, Use of limestone obtained from waste of the mussel cannery industry for the production of mortars, Cem. Concr. Res. 37 (2007) 559–564. doi:10.1016/j.cemconres.2007.01.004.

[8] W.A.S.B.W. Mohammad, N.H. Othman, M.H.W. Ibrahim, M.A. Rahim, S. Shahidan, R.A. Rahman, A review on seashells ash as partial cement replacement, IOP Conf. Ser. Mater. Sci. Eng. 271 (2017) 12059. http://stacks.iop.org/1757-899X/271/i=1/a=012059.

[9] Bouregba, A., Diouri, A., Amor, F., Ez-zaki, H., Sassi, O., Valorization of glass and shell powders in the synthesis of Belitic clinker, MATEC Web Conf. 149 (2018) 1021. doi:10.1051/matecconf/201814901021.

[10] G. Yoon, B. Kim, B. Kim, S. Han, Chemical – mechanical characteristics of crushed oyster-shell, Waste Manag. 23 (2003) 825–834.

[11] H. Yoon, Oyster Shell as Substitute for Aggregate in Mortar, Waste Manag. Res. 22 (2004) 158–170. doi:10.1177/0734242X04042456.

[12] H.Y. Wang, W. Ten Kuo, C.C. Lin, C. Po-Yo, Study of the material properties of fly ash added to oyster cement mortar, Constr. Build. Mater. 41 (2013) 532–537. doi:10.1016/j.conbuildmat.2012.11.021.

[13] S. Motamedi, S. Shamshirband, R. Hashim, D. Petković, C. Roy, Estimating unconfined compressive strength of cockle shell-cement-sand mixtures using soft computing methodologies, Eng. Struct. 98 (2015) 49–58. doi:10.1016/j.engstruct.2015.03.070.

[14] C.F. Liang, H.Y. Wang, Feasibility of pulverized oyster shell as a cementing material, Adv. Mater. Sci. Eng. 2013 (2013). doi:10.1155/2013/809247.

[15] A. Nazari, M. Ghafouri Safarnejad, Prediction early age compressive strength of OPC-based geopolymers with different alkali activators and seashell powder by gene expression programming, Ceram. Int. 39 (2013) 1433–1442. doi:10.1016/j.ceramint.2012.07.086.

[16] P. Lertwattanaruk, N. Makul, C. Siripattarapravat, Utilization of ground waste seashells in cement mortars for masonry and plastering, J. Environ. Manage. 111 (2012) 133–141. doi:10.1016/j.jenvman.2012.06.032.

[17] L. Génio, S. Kiel, M.R. Cunha, J. Grahame, C.T.S. Little, Shell microstructures of mussels (Bivalvia: Mytilidae: Bathymodiolinae) from deep-sea chemosynthetic sites: Do they have a phylogenetic significance?, Deep. Res. Part I Oceanogr. Res. Pap. 64 (2012). doi:10.1016/j.dsr.2012.02.002.

[18] C. Martínez-García, B. González-Fonteboa, F. Martínez-Abella, D. Carro- López, Performance of mussel shell as

aggregate in plain concrete, Constr. Build. Mater. 139 (2017) 570–583. doi:10.1016/j.conbuildmat.2016.09.091.

[19] K. Kochova, K. Schollbach, F. Gauvin, H.J.H. Brouwers, Effect of saccharides on the hydration of ordinary Portland cement, Constr. Build. Mater. 150 (2017) 268–275. doi:10.1016/J.CONBUILDMAT.2017.05.149.

[20] J.C. Mendes, T.K. Moro, A.S. Figueiredo, K.D. do C. Silva, G.C. Silva, G.J.B. Silva, R.A.F. Peixoto, Mechanical, rheological and morphological analysis of cement-based composites with a new LAS-based air entraining agent, Constr. Build. Mater. 145 (2017) 648–661. doi:10.1016/J.CONBUILDMAT.2017.04.024.

[21] A. Sepulcre-Aguilar, Influencia de las Adiciones Puzolánicas en los morteros de restauración de fábricas de interés Historico-Artistico, Universidad Politécnica de Madrid, 2005. http://oa.upm.es/264/1/Alberto_Sepulcre.pdf.

[22] A. Acosta, E. Herrero, J.R. Rosell, D. Sanz, Guía práctica para los morteros con cal, in: 2011.

[23] C. Del Olmo Rodríguez, Los morteros. Control de calidad, Inf. La Construcción. 46 (1994) 57–73. doi:10.3989/ic.1994.v46.i433.1117.

[24] European Parliament and Council, Regulation (EC) No 1069/2009, Off. J. Eur. Union. 300 (2009) 1–33.

[25] AENOR, UNE-EN 1097-6, Tests for mechanical and physical properties of aggregates. Part 6: Determination of particle density and water absorption., (2006).

[26] AENOR, UNE-EN 1744-1,Tests for chemical properties of aggregates. Part 1: Chemical analysis., (2014) 64.

[27] AENOR, UNE 103204, Organic matter content of a soil by the potassium permanganate method., (1993) 4.

[28] AENOR, UNE-EN 933-8. Test for geometrical properties of aggregates. Part 8: Assessment of fines. Sand equivalent test., (2012) 22.

[29] AENOR, UNE-EN 1015-11, Methods of test for mortar for masonry. Part 11: Determination of flexural and compressive strength of hardened mortar., (2007) 8.

[30] AENOR, UNE-EN 1015-10, Methods of test for mortar for masonry. Part 10: Determination of dry bulk density of hardened mortar., 2000.

[31] AENOR, UNE-EN 1015-18, Methods of test for mortar for masonry. Part 18: Determination of water absorption coefficient due to capillary action of hardened mortar., (2003) 11.

[32] AENOR, UNE-EN 12808-4, Grouts for tiles. Part 4: Determination of shrinkage., 2010.

[33] AENOR, UNE-EN 413-2, Masonry cement. Part 2: Test methods., (2006) 20.

[34] AENOR, UNE-EN 1015-9, UNE-EN 1015-9, Methods of test for mortar for masonry. Part 3: Determination of consistence of fresh mortar (by flow table)., 2007.

[35] AENOR, UNE 83980, Concrete durability. Test methods. Determination of the water absorption, density and accessible porosity for water in concrete, 2014.

[36] E.-I. Yang, S.-T. Yi, Y.-M. Leem, Effect of oyster shell substituted for fine aggregate on concrete characteristics: Part I. Fundamental properties, Cem. Concr. Res. 35 (2005). doi:10.1016/j.cemconres.2005.03.016.

[37] B. Safi, M. Saidi, A. Daoui, A. Bellal, A. Mechekak, K. Toumi, The use of seashells as a fine aggregate (by sand substitution) in self-compacting mortar (SCM), Constr. Build. Mater. 78 (2015) 430–438. doi:10.1016/j.conbuildmat.2015.01.009.

[38] M. Khudhair, B. el hilal, A. Elharfi, Review on chemical (organic) admixtures in the cementitious materials, 2018. doi:10.26872/jmes.2018.9.6.192.

[39] M. Lasheras-Zubiate, I. Navarro-Blasco, J.M. Fernández, J.I. Álvarez, Effect of the addition of chitosan ethers on the fresh state properties of cement mortars, Cem. Concr. Compos. 34 (2012) 964–973. doi:10.1016/J.CEMCONCOMP.2012.04.010.

[40] M.A. Salas, J. Gadea, S. Gutiérrez-González, M. Horgnies, V. Calderón, Recycled polyamide mortars modified with non-ionic surfactant: physical and mechanical strength after durability tests, Mater. Struct. 49 (2016) 3385–3395. doi:10.1617/s11527-015-0726-z.

[41] A. Uğur Ozturk, R. Tuğrul Erdem, Influence of the air-entraining admixture with different superplasticizers on the freeze-thaw resistance of cement mortars | Influenţa aditivului antrenor de aer combinat cu diferiti superplastifianţi asupra rezistenţei la îngheţ – dezgheţ a mortarelor de, Rev. Rom. Mater. Rom. J. Mater. 46 (2016).

[42] B.R. Etuk, I.F. Etuk, L.O. Asuquo, Feasibility of Using Sea Shells Ash as Admixtures for Concrete, J. Environ. Sci. Eng. A Former. Part J. Environ. Sci. Eng. 1 (2012) 121–127.

[43] F. Soltanzadeh, M. Emam-Jomeh, A. Edalat-Behbahani, Z. Soltan-Zadeh, Development and characterization of blended cements containing seashell powder, Constr. Build. Mater. 161 (2018) 292–304. doi:10.1016/J.CONBUILDMAT.2017.11.111.

[44] X. Pang, P. Boontheung, P.J. Boul, Dynamic retarder exchange as a trigger for Portland cement hydration, Cem. Concr. Res. 63 (2014) 20–28. doi:10.1016/J.CEMCONRES.2014.04.007.

[45] I.B. Topcu, O. Atesin, T. Uygunoglu, Effect of High Dosage Air-Entraining Admixture Usage on Micro Concrete Properties, EJENS (European J. Eng. Nat. Sci. (2017).

[46] R.K. Takesue, C.R. Bacon, J.K. Thompson, Influences of organic matter and calcification rate on trace elements in aragonitic estuarine bivalve shells, Geochim. Cosmochim. Acta. 72 (2008) 5431–5445. doi:10.1016/J.GCA.2008.09.003.

[47] P. Dalbeck, J. England, M. Cusack, M. Lee, A.E. Fallick, Crystallography and chemistry of the calcium carbonate polymorph switch in M. edulis shells, 2006. doi:10.1127/0935-1221/2006/0018-0601.

[48] Y. Dauphin, J. Cuif, J. Doucet, M. Salomé, J. Susini, C. Williams, In situ mapping of growth lines in the calcitic prismatic layers of mollusc shells using X-ray absorption near-edge structure (XANES) spectroscopy at the sulphur K-edge, Mar. Biol. 142 (2003) 299–304. doi:10.1007/s00227-002-0950-2.

[49] P.E. Hare, Amino acids in the proteins from aragonite and calcite in the shells of Mytilus californianus, Science (80-.). 139 (1963) 216–217. doi:10.1126/science.139.3551.216.

[50] B. Belhadj, M. Bederina, N. Montrelay, J. Houessou, M. Quéneudec, Effect of substitution of wood shavings by barley straws on the physico-mechanical properties of lightweight sand concrete, Constr. Build. Mater. 66 (2014) 247–258. doi:10.1016/J.CONBUILDMAT.2014.05.090.

[51] H. Binici, M. Eken, M. Dolaz, O. Aksogan, M. Kara, An environmentally friendly thermal insulation material from sunflower stalk, textile waste and stubble fibres, Constr. Build. Mater. 51 (2014) 24–33. doi:10.1016/J.CONBUILDMAT.2013.10.038.

[52] M.J. John, S. Thomas, Biofibres and biocomposites, Carbohydr. Polym. 71 (2008) 343–364. doi:10.1016/J.CARBPOL.2007.05.040.

[53] M. Bishop, A.R. Barron, Cement hydration inhibition with sucrose, tartaric acid, and lignosulfonate: Analytical and spectroscopic study, Ind. Eng. Chem. Res. 45 (2006) 7042–7049. doi:10.1021/ie060806t.

[54] N.B. Milestone, The effect of glucose and some glucose oxidation products on the hydration of tricalcium aluminate, Cem. Concr. Res. 7 (1977) 45–52. doi:10.1016/0008-8846(77)90007-2.

[55] N.L. Thomas, J.D. Birchall, The retarding action of sugars on cement hydration, Cem. Concr. Res. 13 (1983) 830–842. doi:10.1016/0008-8846(83)90084-4.

[56] S. Yasuda, K. Ima, Y. Matsushita, Manufacture of wood-cement boards VII: cement-hardening inhibitory compounds of hannoki (Japanese alder,Alnus japonica Steud.), J. Wood Sci. 48 (2002) 242–244. doi:10.1007/BF00771375.

[57] E. Ortega, O. Rodríguez-Martínez, M. Figueroa-Labastida, A.A. Villa-Pulido, A. Sánchez-Fernández, R. Cué-Sampedro, M.A. Gracia-Pinilla, J.L. Menchaca, Long-term influence of chitin concentration on the resistance of cement pastes determined by atomic force microscopy, Phys. Status Solidi. 213 (2016) 3110–3116. doi:10.1002/pssa.201600105.

[58] J. Young, The influence of sugars on the hydration of tricalcium aluminate, in: Proc. 5th Int. Symp. Chem. Cem., Tokyo, 1968: pp. 256–267.

[59] A.I. Rashed, R.B. Williamson, Microstructure of entrained air voids in concrete, Part I, J. Mater. Res. 6 (1991) 2004–

2012. doi:10.1557/JMR.1991.2004.

[60] W. Piasta, H. Sikora, Effect of air entrainment on shrinkage of blended cements concretes, Constr. Build. Mater. 99 (2015) 298–307. doi:10.1016/J.CONBUILDMAT.2015.09.018.

[61] F. Gong, D. Zhang, E. Sicat, T. Ueda, Empirical Estimation of Pore Size Distribution in Cement , Mortar , and Concrete, 26 (2014) 1–11. doi:10.1061/(ASCE)MT.1943-5533.0000945.

[62] J. Lanas, J.L.P. Bernal, M.A. Bello, J.I.A. Galindo, Mechanical properties of natural hydraulic lime-based mortars, Cem. Concr. Res. 34 (2004) 2191–2201. doi:10.1016/j.cemconres.2004.02.005.

[63] M. Arandigoyen, J.L.P. Bernal, M.A.B. López, J.I. Alvarez, Lime-pastes with different kneading water: Pore structure and capillary porosity, Appl. Surf. Sci. 252 (2005) 1449–1459. doi:10.1016/j.apsusc.2005.02.145.

[64] AENOR, UNE-EN 998-1, Specification for mortar for masonry. Part 1: Rendering and plastering mortar., (2010) 26.

[65] R. V. Silva, J. De Brito, R.K. Dhir, Performance of cementitious renderings and masonry mortars containing recycled aggregates from construction and demolition wastes, Constr. Build. Mater. 105 (2016) 400–415. doi:10.1016/j.conbuildmat.2015.12.171.

[66] C.P. Woon, P.N. Shek, M.M. Tahir, A.B.H. Kueh, Compressive Strength of Ground Waste Seashells in Cement Mortars for Masonry and Plastering, in: Front. Mech. Eng. Mater. Eng. III, Trans Tech Publications, 2015: pp. 167–170. doi:10.4028/www.scientific.net/AMM.727-728.167.

[67] H. Ez-zaki, B. El Gharbi, A. Diouri, Development of eco-friendly mortars incorporating glass and shell powders, Constr. Build. Mater. 159 (2018) 198–204. doi:10.1016/J.CONBUILDMAT.2017.10.125.

[68] G. Li, X. Xu, E. Chen, J. Fan, G. Xiong, Properties of cement-based bricks with oyster-shells ash, J. Clean. Prod. 91 (2015) 279–287. doi:10.1016/j.jclepro.2014.12.023.

[69] I. Martínez, M. Etxeberria, E. Pavón, N. Díaz, A comparative analysis of the properties of recycled and natural aggregate in masonry mortars, Constr. Build. Mater. 49 (2013) 384–392. doi:10.1016/j.conbuildmat.2013.08.049.

[70] W. Ten Kuo, H.Y. Wang, C.Y. Shu, D.S. Su, Engineering properties of controlled low-strength materials containing waste oyster shells, Constr. Build. Mater. 46 (2013) 128–133. doi:10.1016/j.conbuildmat.2013.04.020.

[71] J. Jasiczak, K. Zielinski, Effect of protein additive on properties of mortar, Cem. Concr. Compos. 28 (2006) 451–457. doi:10.1016/j.cemconcomp.2005.12.007.